

A Computational Model for Enhanced Accuracy of Radial Harmonic Fourier Moments

C. Singh and R. Upneja

Abstract— Radial Harmonic Fourier Moments (*RHFM*s) are one of the best rotation invariant orthogonal moments which are used in many pattern recognition and image processing applications. They are preferred over Zernike moments (*ZM*s) because of their computational efficiency. Like *ZM*s, the existing approach for the computation of *RHFM*s suffers from two major errors- the geometric error and the numerical integration error. We propose a computational framework based on Gaussian numerical integration which reduces both errors. The proposed approach is as simple as the existing approach in terms of its implementation. The enhanced accuracy of *RHFM*s results in better image reconstruction and improvement in rotation and scale invariance.

Index Terms— Radial harmonic Fourier moments; Geometric error; Numerical integration error; Rotation invariance; Scale invariance.

I. INTRODUCTION

Invariance of features in the presence of basic transformations is a basic requirement in many image processing applications. There are various radial moment based methods which can identify a pattern in terms of certain features. Some of these moments like the Zernike moments (*ZM*s), Pseudo Zernike moments (*PZM*s), Orthogonal Fourier–Mellin moments (*OFMM*s) and Radial Harmonic Fourier Moments (*RHFM*s) possess the property of being invariant to rotation and can be made invariant to translation and scale after geometric transformations [1]. *RHFM*s are better rated in comparison with other moments because they are less computational intensive as compared to other moments [2]. These moments also satisfy the orthogonality condition. Orthogonality of the kernels means that an image is projected onto a set of pairwise orthogonal axes, hence the overlapping of information is minimal. The orthogonality property also enables the separation of individual contribution of moment of each order to the image reconstruction process. Therefore, the number of moments required to reconstruct an image is much less than those obtained from non-orthogonal kernels. Due to these characteristics, *RHFM*s are popular with various applications like image reconstruction [1], character reconstruction [2], image recognition [3], cell image recognition [4], tumor cell recognition [5], image description [6], etc.

The conventional direct method which depends on zeroth order approximation produces geometric error and numerical integration error in *RHFM*s calculation, which is

a common problem with the radial moments. Therefore, using the existing computation method, some of the moments magnitudes are not truly rotationally invariant. Furthermore, the existing errors have such a negative impact on the image analysis and reconstruction that when the order of moments reaches a high value, the resulting reconstruction error becomes intolerable. By inscribing the circle inside square image, the information loss occurs due to the inexact approximation of the circular boundary of the image [2]. To overcome the geometric error, Wee and Paramesran [7] proposed an alternative mapping technique for *ZM*s in which the complete image is contained inside the unit disk. Therefore, all pixels are involved in the computation of radial moments. However, this enhances the domain of calculation. The second source of error arises from sampling the kernel functions of moments at pixel center, which is referred to as the numerical integration error. The higher order moments which are mainly affected by numerical integration error, are required for better representation of an image and for its accurate reconstruction. The geometric error and numerical integration error are more pronounced in small images. Therefore, applications such as optical character recognition and template matching in which small images are used, are more prone to these errors when *RHFM*s are used as features. Numerical instability is another problem which is observed in moment calculation. Numerical instability occurs when the images are small and moment orders are high. The traditional zeroth order approximation of *RHFM*s calculation makes *RHFM*s numerically instable for moment order $p_{\max} > 10$ for inscribed disk and $p_{\max} > 20$ for outer disk for 64×64 pixel images.

In this paper, we propose a novel approach for accurate calculation of *RHFM*s by using numerical integration technique, which not only reduces the numerical integration error but also reduces geometric error for inscribed circular disk. We prefer Gaussian quadrature method over other numerical integration techniques as it is one of the best numerical integration techniques which provides more accurate solution as compared to any other numerical integration for the same number of sampling points [8]. Recently, we have applied numerical integration techniques for the accurate computation of *ZM*s [9]. The enhanced accuracy of *ZM*s results in its improved invariance and image reconstruction. Motivated by the success of accurate computation of *ZM*s, we extend the method to *RHFM*s. The *RHFM*s possess distinct advantage over *ZM*s in terms of computation efficiency. Therefore, in applications where the accuracy and speed are the major considerations the accurate computation of *RHFM*s becomes indispensable in many image processing applications.

The rest of the paper is structured as follows. Section II provides an overview of the *RHFM*s and the existing

Manuscript received March 6, 2012.

C. Singh, Professor, Department of Computer Science, Punjabi University, Patiala, India. E-mail: chandan.csp@gmail.com

R. Upneja, Senior Research Fellow, Department of Computer Science, Punjabi University, Patiala, India, E-mail: rahulupneja@gmail.com

common approach for its computation. The proposed accurate computation of RHFM's is discussed in Section III. Detail experimental results showing the improvement in the performance of the proposed approach are illustrated in Section IV. Conclusion is given in Section V.

II. RADIAL HARMONIC FOURIER MOMENTS

The RHFM's of order p and repetition q with $p \geq 0$ and $|q| \geq 0$ for a continuous function $f(r, \theta)$ over a unit disk are defined as [2]

$$M_{pq} = \frac{1}{2\pi} \int_0^{2\pi} \int_0^1 f(r, \theta) V_{pq}^*(r, \theta) r dr d\theta \quad (1)$$

where $V_{pq}^*(r, \theta)$ is the complex conjugate of $V_{pq}(r, \theta)$ of order p and repetition q , and

$$V_{pq}(r, \theta) = R_p(r) e^{jq\theta} \quad (2)$$

The radial kernel functions are defined by

$$R_p(r) = \begin{cases} \frac{1}{\sqrt{r}}, & p=0 \\ \sqrt{\frac{2}{r}} \cos(\pi p r), & p=\text{even} \\ \sqrt{\frac{2}{r}} \sin(\pi(p+1)r), & p=\text{odd} \end{cases} \quad (3)$$

The orthogonal property for radial kernel is given as

$$\int_0^1 R_p(r) R_k(r) r dr = \delta_{pk} \quad (4)$$

The orthogonality of basis function is given as

$$\int_0^{2\pi} \int_0^1 V_{pq}(r, \theta) V_{p'q'}^*(r, \theta) r dr d\theta = 2\pi \delta_{pp'} \delta_{qq'} \quad (5)$$

for $p=p_{\max}$, the total number of RHFM's is $(1+p_{\max})(1+2q_{\max})$.

In digital image processing, the image function $f(r, \theta)$ is discrete and defined in a rectangular domain with the pixel locations identified by the row and column arrangement. Let (i, k) be a pixel, the index i denotes the row position and k the column, with $i, k = 0, 1, \dots, N-1$, where the resolution of the image is $N \times N$ pixels. The top left corner of the rectangular domain represents the origin $(0,0)$ of the image. We map the pixel location (i, k) into the coordinates within the unit disk using the following transformation

$$x_i = \frac{2i+1-N}{D}, y_k = \frac{2k+1-N}{D}, i, k = 0, 1, \dots, N-1 \quad (6)$$

where

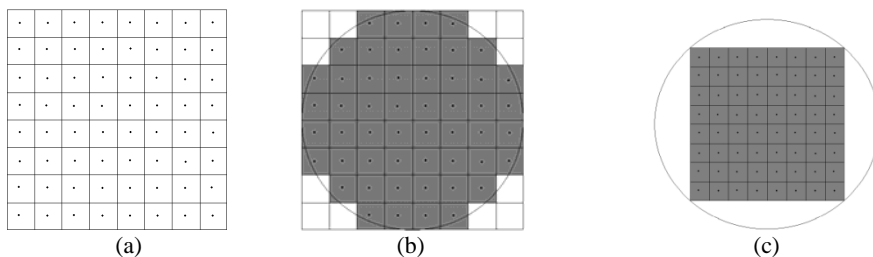


Fig.1: (a) An 8×8 image grid, (b) inscribed circle approximated by square grids, (c) outer circle containing the whole square image.

$$D = \begin{cases} N & \text{for inscribed circular disk contained} \\ & \text{in the square image} \\ N\sqrt{2} & \text{for outer circular disk containing} \\ & \text{the whole square image} \end{cases} \quad (7)$$

The coordinate (x_i, y_k) represents the center of the (i, k) pixel grid with the two opposite vertices defined by $\left[x_i - \frac{\Delta x}{2}, y_k - \frac{\Delta y}{2}\right] \times \left[x_i + \frac{\Delta x}{2}, y_k + \frac{\Delta y}{2}\right]$ where Δx and Δy represent the horizontal and vertical separation between the centers of two pixels which are expressed as

$$\Delta x = \Delta y = \frac{2}{D} \quad (8)$$

The RHFM's can now be described in the Cartesian coordinates and their discrete formulation can be facilitated by converting Eq.(1) into Cartesian system defined by

$$M_{pq} = \frac{1}{2\pi} \iint_{x_i^2 + y_k^2 \leq 1} f(x, y) V_{pq}^*(x, y) dx dy \quad (9)$$

Equation (9) can be derived from Eq.(1) after replacing $r = \sqrt{x^2 + y^2}$ and θ by $\tan^{-1}(y/x)$. The discrete implementation of Eq.(9) assumes the form

$$M_{pq} = \frac{1}{2\pi} \sum_{i=0}^{N-1} \sum_{k=0}^{N-1} f(x_i, y_k) \iint_{x_i^2 + y_k^2 \leq 1} V_{pq}^*(x, y) dx dy \quad (10)$$

It is difficult to derive an analytical solution to the double integration on the r.h.s of Eq. (10), therefore, normally a zeroth order approximation is considered for its evaluation. This leads to

$$M_{pq} = \frac{4}{2\pi D^2} \sum_{i=0}^{N-1} \sum_{k=0}^{N-1} f(x_i, y_k) V_{pq}^*(x_i, y_k) \quad (11)$$

When $D = N$, then the inscribed disk is used for the computation and some of the pixels whose centers fall outside the disk are left out in the process of moment calculation. This results in what is commonly known as the geometric error. The zeroth order approximation of the double integration leads to another error called the numerical integration error. The geometric error is eliminated when the outer disk enclosing the complete square image is considered which is represented by taking $D = N\sqrt{2}$, because for this computational framework the condition $x_i^2 + y_k^2 \leq 1$ is satisfied for all image pixels. The two conditions, i.e., $D = N$ and $D = N\sqrt{2}$, are elaborated in Fig. 1, where Fig.1(a) represents an 8×8 image grid, Fig.1(b) depicts the mapping of image pixels for $D = N$, and Fig.1(c) represents the case when $D = N\sqrt{2}$. Clearly, in Fig.1(b) some of the image pixels which do not satisfy the condition $x_i^2 + y_k^2 \leq 1$ are left out in the process of moment computation.

Suppose that moments of all orders $p \leq p_{\max}$ and repetition $q \leq q_{\max}$ are given, then the image is reconstructed as follows

$$\hat{f}(x_i, y_k) = \sum_{p=0}^{p_{\max}} \sum_{q=0}^{q_{\max}} M_{pq} V_{pq}(x_i, y_k), i, k=0, 1, \dots, N-1 \quad (12)$$

The image reconstruction error ε is defined by

$$\varepsilon = \frac{\sum_{i=0}^{N-1} \sum_{k=0}^{N-1} (f(x_i, y_k) - \hat{f}(x_i, y_k))^2}{\sum_{i=0}^{N-1} \sum_{k=0}^{N-1} f^2(x_i, y_k)} \quad (13)$$

III. ACCURATE COMPUTATION OF RHFMS

The zeroth order approximation of the double integration leads to numerical integration error. The magnitude of the numerical integration error is not known. However, it is expected to be high for high orders of p and q . We analyze this fact by noting that the kernel functions of *RHFM*s are sinusoidal functions which have $2p$ number of zeros in the interval $r \in [0,1]$ for the radial kernels and $2q$ number of zeros for the angular functions for $\theta \in [0, 2\pi]$. When p or q is high the rate of change of function in the interval $[0,1]$ or $[0, 2\pi]$ will be proportionally high. This trend is depicted in Fig.2 which demonstrates the variation of $R_p(r)$ w.r.t. r for various values of p . Another important characteristics of the radial kernel function is their singular behavior at $r=0$. These characteristics lead to the inaccuracy and numerical instability in the computation of *RHFM*s especially for the high values of p and q . In order to alleviate these problems we resort to the numerical integration of the kernel functions. There are several methods for the numerical integration but it is reported that the Gaussian quadrature method is the best method [8]. Let $f(x)$ be an 1-D function, then its numerical integration in the interval $[a,b]$ is given by

$$\int_a^b f(x) dx \cong \frac{(b-a)}{2} \sum_{i=0}^{n-1} w_i f\left(\frac{a+b}{2} + \frac{b-a}{2} t_i\right) \quad (14)$$

where w_i and t_i are the known weights and the location of sampling points and n is the order of the numerical integration. There are standard procedures to find the values of w_i and t_i for a given n [8]. The values of w_i are fixed and $\sum_{i=0}^{n-1} w_i = 2$. The values of t_i can be expressed in terms of the limits of the integration a and b . For a quick reference we provide these values in Table 1 for $n=1$ through 10. It may be noted that for $n=1$, the zeroth order approximation of the integration is obtained. The 2-D formulation of the numerical integration of $f(x, y)$ is expressed as

$$\iint_{a,c}^{b,d} f(x, y) dx dy \cong \frac{(b-a)(d-c)}{4} \times \sum_{l=0}^{n-1} \sum_{m=0}^{n-1} w_l w_m f\left(\frac{a+b}{2} + \frac{b-a}{2} t_l, \frac{c+d}{2} + \frac{d-c}{2} t_m\right) \quad (15)$$

We can now accurately compute *RHFM*s by resorting to Gaussian numerical integration of the double integration in Eq.(10)

$$M_{pq} \cong \frac{1}{2\pi D^2} \sum_{i=0}^{N-1} \sum_{k=0}^{N-1} f(x_i, y_k) \times \sum_{l=0}^{n-1} \sum_{m=0}^{n-1} w_l w_m V_{pq}^*\left(\frac{t_l + 2i + 1 - N}{D}, \frac{t_m + 2k + 1 - N}{D}\right), \left(\frac{t_l + 2i + 1 - N}{D}\right)^2 + \left(\frac{t_m + 2k + 1 - N}{D}\right)^2 \leq 1 \quad (16)$$

The constraint given in Eq.(16) is an improvement over the constraint $x_i^2 + y_k^2 \leq 1$ used in the zeroth order approximation for inscribe circular disk. This constraint also allows those grids to take part in computation whose center fall outside the circle but the sampling point fall within the unit disk. It is also interesting to observe that the implementation of Eq.(16) is as simple as Eq.(11) except for the two extra summation operations which account for the new sampling locations.

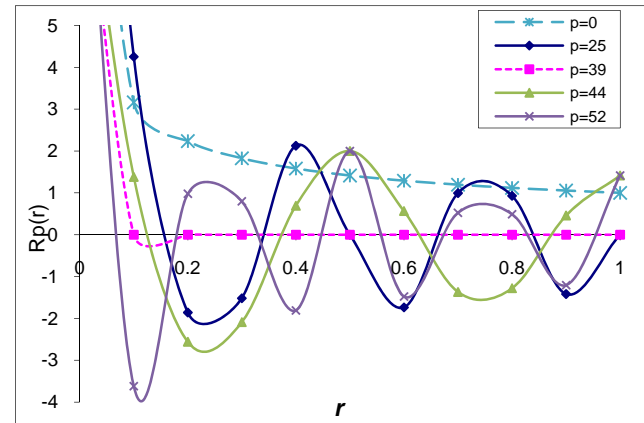


Fig. 2: $R_p(r)$ of *RHFM*s for various orders p .

Table 1 Weights and location of sampling points for $n \times n$ point Gaussian integration.

n	w_i	t_i	n	w_i	t_i
1	2.0	0.0	8	0.10122853	± 0.96028987
2	1.0	± 0.57735027		0.22238103	± 0.79666648
3	0.55555556	± 0.77459667		0.31370665	± 0.52553241
	0.88888889	0.0		0.36268378	± 0.18343464
4	0.34785485	± 0.86113631	9	0.08127439	± 0.96816024
	0.65214515	± 0.33998104		0.18064816	± 0.83603111
5	0.23692688	± 0.90617985		0.26061070	± 0.61337143
	0.47862867	± 0.53846931	10	0.31234708	± 0.32425342
	0.56888889	0.0		0.33023935	0.0
6	0.17132449	± 0.93246951	10	0.06667134	± 0.97390653
	0.36076157	± 0.66120939		0.14945135	± 0.86506337
	0.46791393	± 0.23861919		0.21908636	± 0.67940957
7	0.12948497	± 0.94910791	10	0.26926672	± 0.43339539
	0.27970539	± 0.74153119		0.29552422	± 0.14887434
	0.38183005	± 0.40584515			
	0.41795918	0.0			

IV. EXPERIMENTAL ANALYSIS

The computational framework presented in this paper is implemented in Visual C++6.0 under Windows environment on a PC with 3.0 GHz CPU and 3GB RAM. We take twelve standard gray scale images which are normally used for various image processing analysis [7]. The images which are 256×256 pixels, are resized to 64×64 pixels in order to highlight the effect of geometric and numerical integration error in smaller images. The accuracy of *RHFM*s is measured in terms of image reconstruction capability, reconstruction error, rotation and scale invariance

A. Image Reconstruction and Reconstruction Error

Image reconstruction capability is one of the major characteristics of orthogonal moments. The improvements in

the accuracy of RHFMs can be observed through the quality of reconstructed images. For this purpose computation of RHFMs are performed for 1×1 (zeroth order), 2×2 , 3×3 , 4×4 and 5×5 order of integration. The reconstruction error, ε , as a function of p and q are shown in Fig.3 and 4, for $D = N$ (inscribed circle) and $D = N\sqrt{2}$ (outer circle), respectively. It is shown in the figures that the accuracy in RHFMs increases with the order of integration. The zeroth order integration becomes numerically unstable for $p_{\max} > 10$ for the inscribed circle and $p_{\max} > 20$ for the outer circle. There is a decreasing trend of ε w.r.t. p_{\max} and this decrease is more prominent as n increases. The reconstructed images are shown in Fig.6 and 7 for $n = 1, 3$ and 5 only due to space constraints. The experiments are conducted on 64×64 Pirate image which has high contrast of gray values. Figure 5 displays the original Pirate image. The quality of reconstructed images is far better for the proposed method than the existing method. It can also be observed that the image quality deteriorates in the vicinity of $r = 0$ which is a reflection of the singularity aspect of the kernel function. The instability in RHFMs calculation which is most prominent in the vicinity of $r = 0$ is attributed to the fact that as $r \rightarrow 0$, $R_p(r) \rightarrow \infty$. Thus the magnitude of $R_p(r)$ fluctuates more prominently in the vicinity of $r = 0$ for high values of p . It is seen in Fig.2 that the value of $R_p(r)$ changes rapidly in the vicinity of $r = 0$. The center of the image and its neighborhood are much sensitive to the numerical integration error. Thus, it is observed that the numerical integration error is a prominent source of error in orthogonal RHFMs computation and it increases as the orders of moments increase, which results in the degradation of the reconstructed images. It is also worth mentioning here that while the reconstruction error ε reflects the gross behavior of the error, the visual aspect of reconstructed images represents the local trend in the accuracy of RHFMs.

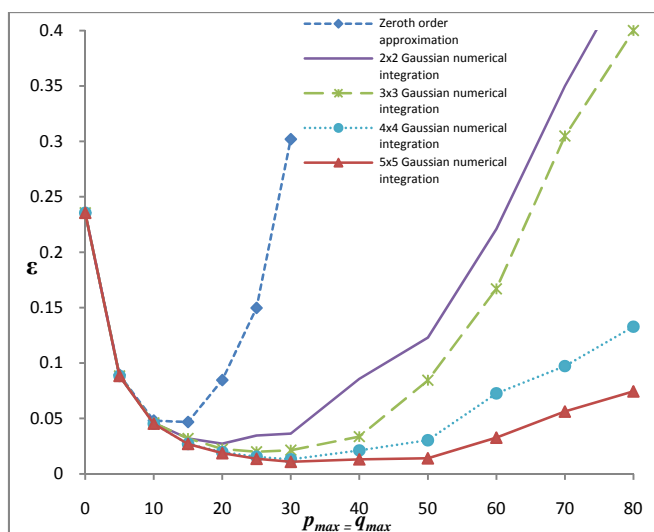


Fig.3: Average mean square reconstruction error ε as a function of order of moments for twelve standard images of 64×64 pixels (inscribed circle).

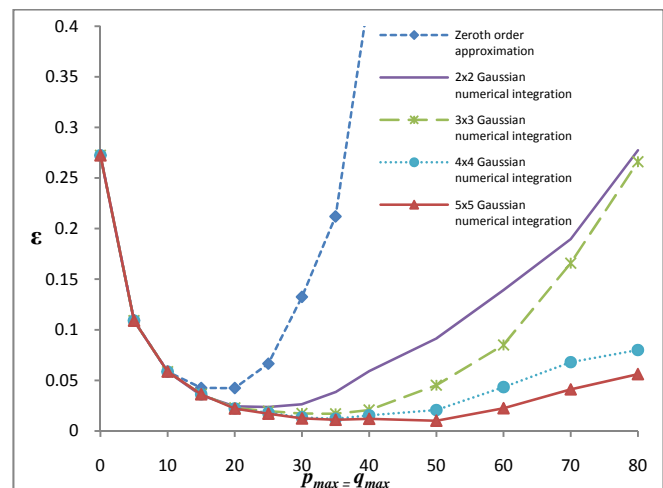


Fig.4: Average mean square reconstruction error ε as a function of order of moments for twelve standard images of 64×64 pixels (outer circle).



Fig.5: Pirate 64×64 image (one of the standard images of size 256×256 pixels which is resized to 64×64 pixels).

$p_{\max} = q_{\max}$	Zeroth order approximation	3x3 Gaussian numerical integration	5x5 Gaussian numerical integration
10	 $\varepsilon=0.050292$	 $\varepsilon=0.047930$	 $\varepsilon=0.047469$
20	 $\varepsilon=0.049224$	 $\varepsilon=0.020363$	 $\varepsilon=0.018198$
30	 $\varepsilon=0.119067$	 $\varepsilon=0.013610$	 $\varepsilon=0.009667$
40	 $\varepsilon=0.401417$	 $\varepsilon=0.015384$	 $\varepsilon=0.009254$
50	 $\varepsilon=1.414290$	 $\varepsilon=0.032905$	 $\varepsilon=0.007926$
60	 $\varepsilon=4.688779$	 $\varepsilon=0.057156$	 $\varepsilon=0.014824$

Fig.6: Reconstructed image of Pirate 64×64 using RHFMs, with different orders, $p_{\max} = q_{\max} = 10$ to 60 for inscribed circle.





$p_{\max} = q_{\max}$	Zeroth order approximation	3×3 Gaussian numerical integration	5×5 Gaussian numerical integration
10	 $\varepsilon = 0.053981$	 $\varepsilon = 0.053212$	 $\varepsilon = 0.053212$
20	 $\varepsilon = 0.031347$	 $\varepsilon = 0.024451$	 $\varepsilon = 0.024184$
30	 $\varepsilon = 0.056314$	 $\varepsilon = 0.015454$	 $\varepsilon = 0.013554$
40	 $\varepsilon = 0.168253$	 $\varepsilon = 0.013607$	 $\varepsilon = 0.009879$
50	 $\varepsilon = 0.408862$	 $\varepsilon = 0.022029$	 $\varepsilon = 0.007523$
60	 $\varepsilon = 1.078854$	 $\varepsilon = 0.034944$	 $\varepsilon = 0.011968$

Fig.7: Reconstructed image of Pirate 64×64 using *RHFM*s, with different orders, $p_{\max} = q_{\max} = 10$ to 60 for outer circle.

B. Rotation and Scale Invariance

Rotation and scale invariance are the most useful characteristics of *RHFM*s. These properties are, however, affected by various errors and the discrete nature of the image function. The magnitudes of *RHFM*s $|M_{pq}|$ remain invariant to rotation, and hence can be used as rotation-invariant features for image representation. In order to analyze the effects of errors on rotation invariance, all twelve standard images are resized to 64×64 pixels and rotated by angles ranging from 0° to 90° with an interval of 10° . In order to evaluate quantitatively the effect of rotation, we define the average mean square error, *MSE*, of *RHFM*s magnitudes as

$$MSE = \frac{1}{L} \sum_{p=0}^{p_{\max}} \sum_{q=0}^{q_{\max}} \left(|M_{pq}^\alpha| - |M_{pq}| \right)^2 \quad (17)$$

where $\alpha = 0^\circ, 10^\circ, 20^\circ, \dots, 90^\circ$ are the angles of rotation set in our experiments, M_{pq} and M_{pq}^α are the *RHFM*s of the non-rotated and rotated images, respectively, and L is the total number of moments for a given maximum order p_{\max} and repetition q_{\max} . We take 3×3 and 5×5 sampling points in

proposed method for invariance analysis. The average *MSE* is plotted for various angles of rotation for the twelve standard images for zeroth order approximation and proposed method by taking $p_{\max} = q_{\max} = 20$ and the results are shown in Fig.8 and Fig.9 corresponding to inscribed circle and outer circle, respectively. We observe that the proposed method provides small values of average *MSE* as compared to zeroth order approximation. This shows that the rotation invariance property is severely affected by the presence of these errors.

Similarly, in order to evaluate quantitatively the effect of scale, we define the average mean square error, *MSE*, of *RHFM*s magnitudes as

$$MSE = \frac{1}{L} \sum_{p=0}^{p_{\max}} \sum_{q=0}^{q_{\max}} \left(|M_{pq}^s| - |M_{pq}| \right)^2 \quad (18)$$

where M_{pq} represents *RHFM*s for the image of the size 64×64 pixels and M_{pq}^s represents the *RHFM*s of an image scaled by a factor s . For this purpose, we resize all 12 images to 64×64 pixels and consider them to be the reference images. The values of *MSE* are computed for all twelve images and their average value is plotted in Figs.10 and 11 for $p_{\max} = q_{\max} = 20$. Again, the accurate method for *RHFM*s calculation provides much better results than the zeroth order approximation.

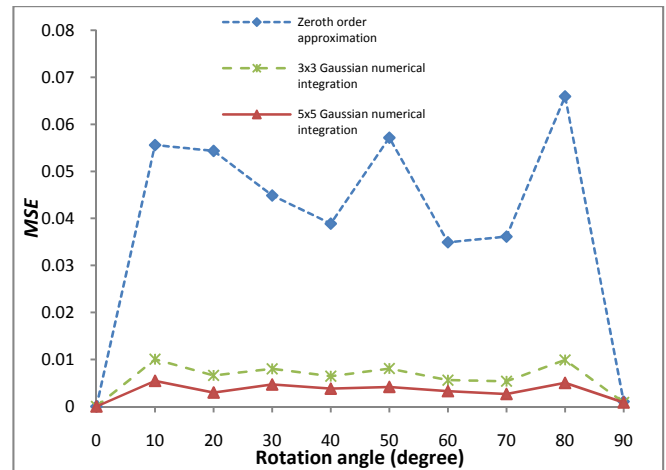


Fig.8: Effect of rotation on average mean square error (*MSE*) of *RHFM*s magnitude for $p_{\max} = q_{\max} = 20$ on 12 standard images (inscribed circle).

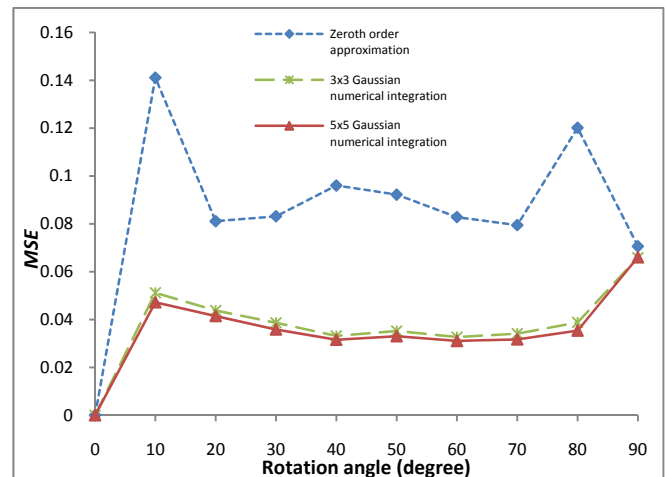


Fig.9: Effect of rotation on average mean square error (*MSE*) of *RHFM*s magnitude for $p_{\max} = q_{\max} = 20$ on 12 standard images (outer circle).

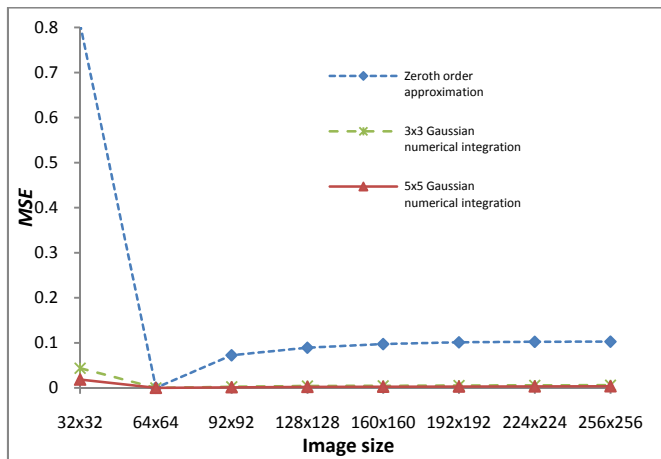


Fig.10: Effect of scale on average mean square error (*MSE*) of *RHFMs* magnitude for $p_{\max} = q_{\max} = 20$ on 12 standard images (inscribed circle).

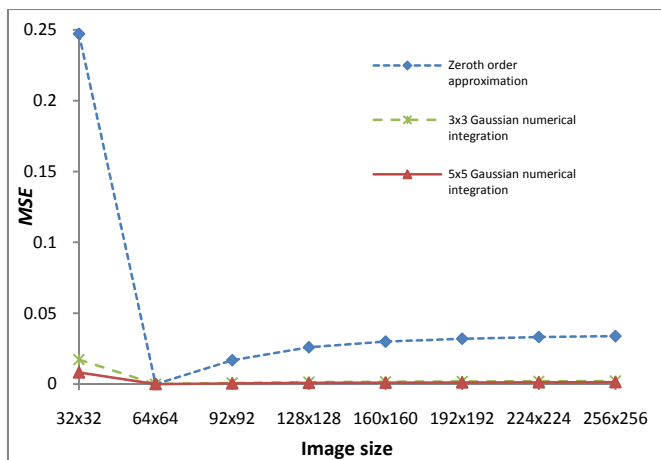


Fig.11: Effect of scale on average mean square error (*MSE*) of *RHFMs* magnitude for $p_{\max} = q_{\max} = 20$ on 12 standard images (outer circle).

V. CONCLUSIONS

The existing method of the computation of RHFMs based on the zeroth order approximation of double integration of the kernel function suffers from geometric error and numerical integration error. The proposed method for the accurate computation of RHFMs reduces both errors with is reflected in the reduction in the image reconstruction error and the quality of the reconstructed images increases significantly. The accuracy in RHFMs also improves the rotation and scale invariance of these moments. The proposed method is particularly useful for pattern matching problems where small images and high computation requirements are involved particularly in the template matching and optical character recognition applications. Thus the advantage of time efficiency which RHFMs provide over their counterparts such as the Zernike moments can be fully utilized in light of the proposed accurate calculation of RHFMs.

REFERENCES

- [1] C. Singh, S. Pooja, R. Upneja, "On Image Reconstruction, Numerical Stability, and Invariance of Orthogonal Radial Moments and Radial Harmonic Transforms," Pattern recognition and image analysis, vol. 21, no. 4, pp. 663–676, 2011.

- [2] H. Ren, A. Liu, J. Zou, D. Bai, Z. Ping, "Character reconstruction with Radial harmonic fourier moments," in Proc. of the 4th Int. Conf. on Fuzzy Systems and Knowledge Discovery 2007 (FSKD07), 3 2007, pp. 307-310.
- [3] H. Ren, Z. Ping, W. Bo, W. Wu, Y. Sheng, "Multidistortion-invariant image recognition with radial harmonic Fourier moments," J. Opt. Soc. Am. A, vol. 20, no. 4, 631-637, 2003.
- [4] R. H. Ping, P. Z. Liang, B. W.-R.-Gen, S. Y. Long, C. S. Zu, W. W.-Kai, "Cell image recognition with Radial harmonic Fourier moments," Chinese Physics, vol. 12, no. 6, pp. 610-614, 2003.
- [5] H. Ren, A. Liu, J. Zou, Z. Ping, D. Bai, "Study on a novel tumor cell recognition system based on orthogonal image moments," in Proc. of 7th Asian-Pacific Conference on Medical and Biological Engineering: APCMBE, Beijing, China, 19, 2008, pp. 290-292.
- [6] T. V. Hoang, S. Tabbone, "Generic Polar Harmonic Transforms for Invariant Image Description, in Proc. Of IEEE International Conference on Image Processing - ICIP," Brussels, Belgium, Sep 2011, pp. 845-848.
- [7] C.Y. Wee, R. Paramseran, "On the computational aspects of Zernike moments, Image and Vision Computing," vol.25, pp. 967-980, 2007.
- [8] J. D. Faires, R. L. Burden, "Numerical Methods," Brooks Cole Publication, 3rd edn., 2002.
- [9] C. Singh, R. Upneja, "Fast and accurate method for high order Zernike moments computation," Appl. Math. Comput., vol. 218, pp. 7759-7773, 2012.